ACS OMEGA

http://pubs.acs.org/journal/acsodf

Article

Study on Screening and Evaluation of Foam Drainage Agents for Gas Wells with High Temperature and High Pressure

Jian Guan, Lihao Liang,* Yulong Zhao, Ning Sun, Wei Lu, and Yuanshui Zhen

Cite This: *ACS Omega* 2023, 8, 7940−7949

Read Online

ACCESS | Metrics & More | Article Recommendations

ABSTRACT: Foam drainage gas recovery technology is a chemical method to solve the serious bottom-hole liquid loading in the middle and late stages of gas well production, and the optimization of foam drainage agents (referred to as FDAs) is the key to the technology. According to the actual reservoir conditions, a high-temperature and high-pressure (HTHP) evaluation device for FDAs was set up in this study. The six key properties of FDAs, such as HTHP resistance, dynamic liquid carrying capacity, oil resistance, and salinity resistance, were evaluated systematically. Taking initial foaming volume, half-life, comprehensive index, and liquid carrying rate as evaluation indexes, the FDA with the best performance was selected and the concentration was optimized. In addition, the experimental results were verified by surface tension measurement and electron microscopy observation. The results showed that the sulfonate compound surfactant (UT-6) had good foamability, excellent foam stability, and better oil resistance at high temperature and high pressure. In addition, UT-6 had stronger liquid carrying capacity at a lower concentration, which could meet the production requirement when the salinity was 80 000 mg/L. Therefore, compared with the other five FDAs, UT-6 was more suitable for HTHP gas wells in block X of the Bohai Bay Basin, whose optimal concentration was 0.25 wt %. Interestingly, the UT-6 solution had the lowest surface tension at the same concentration, with the generated bubbles being closely arranged and uniform in size. Moreover, in the UT-6 foam system, the drainage speed at the plateau boundary was relatively slower with the smallest bubble. It is expected that UT-6 will become a promising candidate for foam drainage gas recovery technology in HTHP gas wells.

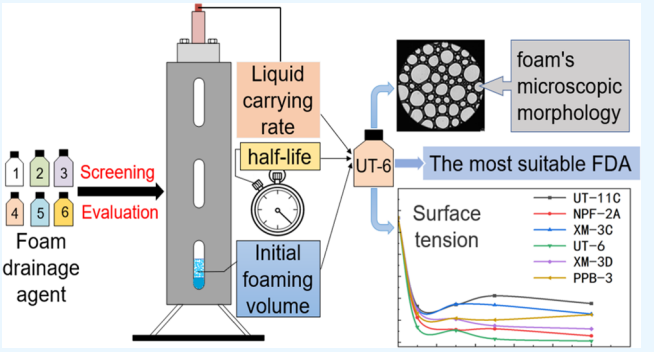

1. INTRODUCTION

Bottom-hole liquid loading is usually an inevitable problem in the production of natural gas wells, which not only restricts the normal production of natural gas wells but also seriously affects the ultimate recovery ratio of gas fields.[1,2] The natural gas exploration and development potential of block X of the Bohai Bay Basin is great; however, compared with other gas fields, the reservoir's physical properties are poor, the original formation pressure is high, and the rock's stress sensitivity is strong. Moreover, the water yield from the formation is high, and once the wellbore begins to accumulate the liquid, the amount of bottom-hole liquid loading will increase rapidly, resulting in serious water lock in the formation around the wellbore.[3] At the same time, with the decrease of permeability, the productivity of gas well will drop rapidly and even the production will stop in a short time.[4] Among them, the problem of bottom-hole liquid loading of high-temperature and high-pressure (HTHP) gas wells in block X is particularly serious. Taking a well in block X as an example, the accumulated gas production of this well is 337.3 × 10^4 m^3, the accumulated oil production is 35 tons, and the accumulated water production is 1635 m^3. The water−gas ratio is large, which is relatively stable in the range of 4−5/10^4 m^3. The current gas-lift drainage method can no longer meet the demand of drainage and gas production, so it is urgent to adopt appropriate technology to discharge the liquid in the bottom hole and improve the production of gas wells.

The common drainage gas recovery technologies mainly include three categories: mechanical method, gas dynamics method, and chemical method.[5−7] The mechanical method mainly includes the plunger gas lift method using an electric submersible pump or a gas acceleration pump for drainage and gas production.[8] The mechanical method has a relatively large daily displacement, a high degree of automation, and wide application, but the initial investment cost and the later management and maintenance costs are relatively high, and

Received: December 3, 2022
Accepted: February 6, 2023
Published: February 16, 2023

https://doi.org/10.1021/acsomega.2c07715
ACS Omega 2023, 8, 7940−7949

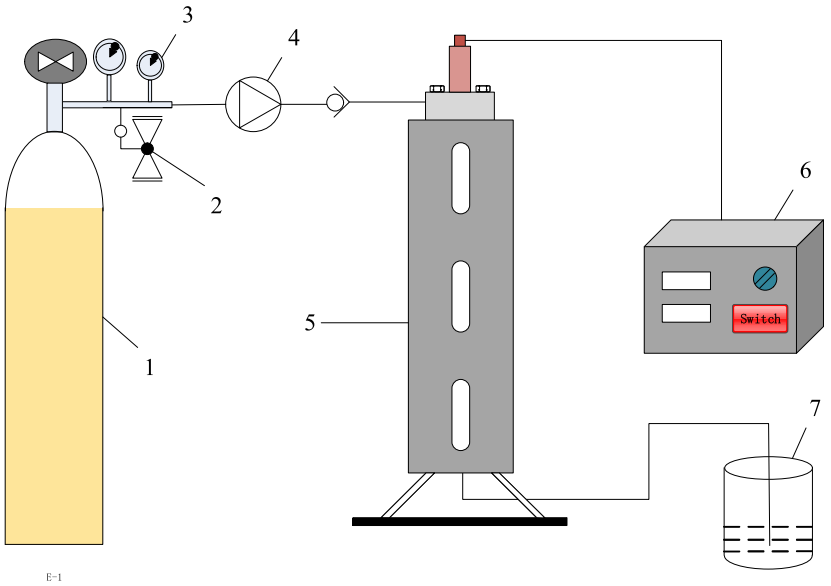

1–nitrogen cylinder; 2–pressure reducing valve; 3–pressure gauge; 4–gas booster pump; 5–HTHP foam evaluation device; 6–control box; 7–liquid collecting bottle

Figure 1. Connection diagram for evaluation of FDA at HTHP.

some technologies are restricted by the depth of the well.[9] At the same time, considering the complicated underground environment, the risk of scaling or corrosion is relatively high.[10] The gas dynamics method is mainly based on velocity string technology, which can be constructed once and does not involve maintenance costs, but its daily displacement is small.[11] The chemical method is mainly based on foam drainage gas recovery technology, which has low investment cost, simple operation process, and can adapt to the complex underground environment.[12] However, the selection of foam drainage agent (FDA) is the core of this technology, and the FDA used should be compatible with formation water and should have strong foamability, foam stability, and liquid carrying capacity in the corresponding formation environment.[13,14]

Considering the actual formation conditions and current production situation of HTHP gas wells, it is more suitable to use foam drainage gas recovery technology to discharge the bottom-hole liquid loading. However, there are few studies on the screening and evaluation of FDAs under HTHP conditions in China at present, so it is necessary to select the most suitable FDA for HTHP gas wells in block X according to the actual formation conditions.

Prior to this, the FDA solution was prepared with simulated formation water, and 100 commonly used FDAs with good performance were preliminarily evaluated under normal temperature and pressure based on the stirring method.[15] Finally, six FDAs with good compatibility with formation water and relatively good foamability and foam stability were selected. The work of this research was to evaluate HTHP resistance, oil resistance, dynamic liquid carrying capacity, and salinity resistance of the six selected FDAs and to screen out the one with the best performance and get the optimum concentration based on the above experimental results. In addition, the experimental results of screening and evaluation were verified by surface tension measurement and electron microscopy observation.[16] By this research, we hope to provide theoretical reference and technical support for the optimization of FDA for HTHP gas wells using foam drainage gas recovery technology.

2. METHOD

2.1. Experimental Materials. Six FDAs used in HTHP evaluation were provided by the Drilling and Production Research Institute, namely, plant soap compound surfactant (UT-11C), nanoparticle high-temperature-resistant FDA (NPF-2A), fatty alcohol poly(oxyethylene) ether ammonium sulfonate (XM-3C), sulfonate compound surfactant (UT-6), low-molecular FDA (XM-3D), and nonionic FDA (PPB-3). In addition, the low-viscosity oil used in oil resistance evaluation was also provided by the Drilling and Production Research Institute. According to the analysis results of the formation water composition of HTHP gas wells in block X, the simulated formation water with a total salinity of 5175.48 mg/L was prepared using chemicals and distilled water in the laboratory.

2.2. Evaluation of HTHP Resistance. According to the Ross–Miles method, the concentration of FDA solution was set to 0.25 wt % with simulated formation water.[17] First, the experimental devices were connected as shown in Figure 1, and 200 mL of FDA solution was poured into the HTHP foam evaluation device. Second, the temperature was set to 120, 130, 140, 150, and 160 °C in turn after the device had been sealed, and a nitrogen cylinder was used to pressurize the device to 1 MPa. Third, after the FDA solution in the device had been stirred at the maximum speed for 2 min, the initial foaming height and foam's half-life were recorded. In addition, the inner diameter of the HTHP foam evaluation device measured using a vernier caliper was 6 cm, so the initial foaming volume could be calculated by multiplying the inner bottom area by the initial foaming height. As for the half-life, it refers to the time it took from the initial foaming volume to half of the initial foaming volume, as shown in Figure 2.

The initial foaming volume reflected the foamability of the FDA, and the half-life reflected the foam stability, which should

https://doi.org/10.1021/acsomega.2c07715
ACS Omega 2023, 8, 7940−7949

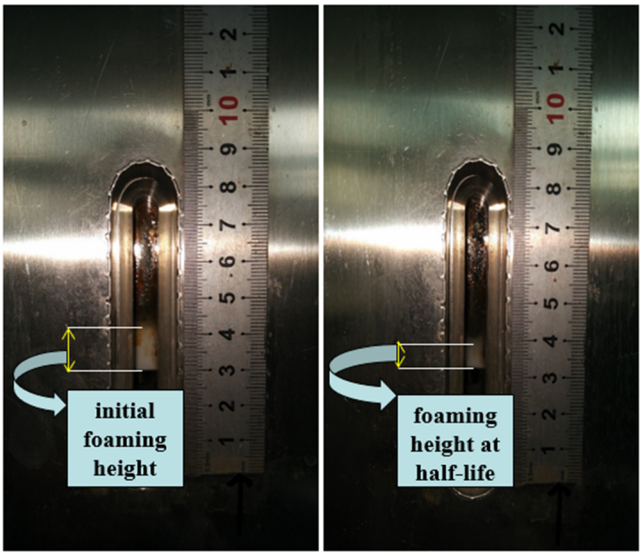

Figure 2. Initial foaming height and foaming height at half-life.

be considered at the same time.[18] Therefore, the comprehensive index was introduced, which was the product of initial foaming volume and half-life, along with a comprehensive evaluation index of foamability and foam stability.[19]

The experimental steps of high-pressure resistance evaluation were basically the same as those of high-temperature resistance evaluation, but they were different in terms of the experimental conditions. The pressure values for high-pressure resistance evaluation were set to 1, 4, 7, and 10 MPa, respectively, and the temperature during high-pressure resistance evaluation was kept constant at 160 °C. The connection diagram is shown in Figure 1, which was the same as the one for high-temperature resistance evaluation.

2.3. Evaluation of Liquid Carrying Capacity. First, six FDA solutions with concentrations of 0.15, 0.25, 0.35, and 0.45 wt % were prepared with simulated formation water, and the experimental devices were connected as shown in Figure 3. Second, 1000 mL of FDA solution with a certain concentration was poured into the HTHP foam evaluation device, and the temperature was set to 160 °C after the device had been sealed. Then, a glass rotor gas flowmeter and a pressure-reducing valve were used to control the gas outlet flow rate to 300 mL/s, and the outlet pressure of the back pressure valve was set to 1 MPa. When the temperature increased to 160 °C, nitrogen was introduced from the bottom of the device at a flow rate of 300 mL/s, and the aeration time was set to 3, 9, and 92.6 min, which corresponded to the water−gas ratio of 1:54, 1:162, and 1:1667 (simulating the actual water−gas ratio in the field), respectively. Finally, the liquid and foam carried out by nitrogen within the set aeration time were collected and allowed to stand until all of the foam was defoamed completely; then, the volume of the liquid in the collecting bottle was recorded, and the liquid carrying rate could be calculated according to the following formula.

$$\text{liquid carrying rate}\ (\%) = \frac{\text{volume of the liquid in the collecting bottle}}{1000} \times 100\%$$

2.4. Evaluation of Oil Resistance. The experimental steps of oil resistance evaluation were basically the same as those of high-temperature resistance evaluation, but they were different in terms of the experimental conditions. The connection diagram is shown in Figure 1, and the temperature was controlled at 160 °C. After 200 mL of FDA solution had been poured into the device, the low-viscosity oil was added to the device corresponding to 5, 15, and 25% of the volume of FDA solution. The other experimental steps and conditions were consistent with those of high-temperature resistance evaluation. The initial foaming volume and half-life were recorded for each experiment.

2.5. Evaluation of Salinity Resistance. After HTHP resistance evaluation, liquid carrying capacity evaluation, and oil resistance evaluation, the best FDA was screened out and its salinity resistance was evaluated. During the early stage of experiments, the total salinity of the simulated formation water used to prepare the FDA solution was 5175.48 mg/L. To find out whether the selected FDA had good anti-high-salinity ability, the FDA solution with a concentration of 0.25 wt % was prepared with simulated formation water with different salinities including 20 000, 35 000, 50 000, 65 000, 80 000, and 95 000 mg/L. Moreover, the other experimental steps were basically the same as those of high-temperature resistance evaluation, and the temperature was controlled at 160 °C. In

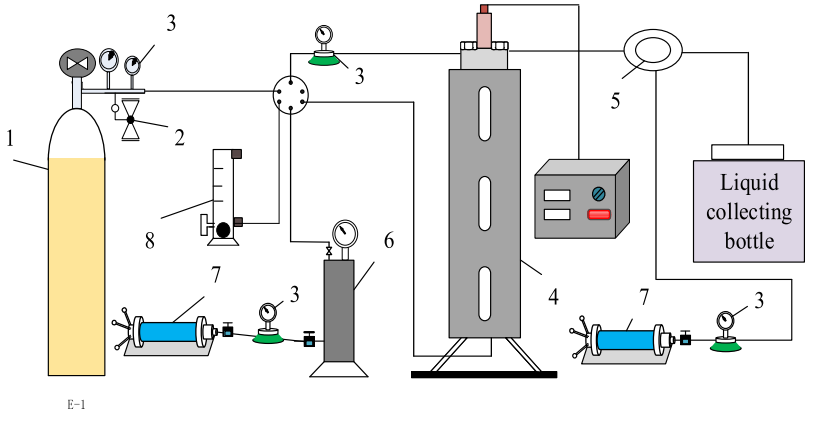

1−nitrogen cylinder; 2−pressure reducing valve; 3−pressure gauge; 4−HTHP foam evaluation device; 5−back pressure valve; 6−pressure vessel; 7−hand pump; 8−glass rotor gas flowmeter

Figure 3. Connection diagram for evaluation of liquid carrying capacity of FDA.

https://doi.org/10.1021/acsomega.2c07715
ACS Omega 2023, 8, 7940−7949

addition to the initial foaming volume and half-life, the liquid carrying rates of FDA with different salinities should also be measured. The experimental steps and conditions were basically the same as those in the evaluation of liquid carrying capacity, and the aeration time was controlled at 9 min.

2.6. Surface Tension Reduction Capacity. With simulated formation water and a 1000 mL volumetric flask, each of the six FDA solutions with concentrations of 0.05, 0.15, 0.25, and 0.5 wt % were prepared. Using simulated formation water without any FDA as a blank sample, the surface tensions of the six FDA solutions with different concentrations were measured using an interfacial tension tester. Because of the limitation of the measuring range, the interfacial tension tester could not work when the temperature exceeded 90 °C. So, the FDA solutions to be measured were heated at 160 °C for 3 days in a drying oven, and then their surface tensions could be measured. First, the FDA solution was injected into a sample tube with a syringe, and a bubble was created with a needle in the middle of the sample tube filled with the FDA solution. Second, the sample tube was placed on the rotating shaft of the main machine after it had been sealed, and the rotating speed was set to 6000 r/min and the experimental temperature was set to 90 °C. When the bubble shape in the sample tube did not change anymore, the surface tension value could be recorded.

2.7. Morphology under an Electron Microscope. According to the previous experimental results, three FDAs with better performance were selected from six for the observation experiment with an electron microscope. The FDA solutions with a concentration of 0.25 wt %, which had been heated at 160 °C in the drying oven for 3 days in the previous experiment, could be directly used. The current experiment was carried out in a constant temperature box at 90 °C, 100 mL of FDA solution was poured into a stirrer and stirred at the maximum rotation speed for 2 min, and then the generated foam was quickly poured into a measuring cylinder, so the initial foaming volume could be read. At the same time, the foam's microscopic morphology was observed and photographed with an electron microscope magnified 100 times. In addition, the foam's microscopic morphology at half-life and double half-life should also be observed and photographed.

3. RESULTS AND DISCUSSION

3.1. High-Temperature Resistance. The relationship of initial foaming volume, half-life, and comprehensive index with temperature is shown in Figures 4–6, respectively. It could be seen from the figures that with the increase of temperature, the initial foaming volume and half-life of the six FDAs all decreased, indicating that high temperature would inhibit the foamability and foam stability. On the one hand, with higher viscosity of the liquid phase, the liquid flow on the surface of foam liquid film became more difficult, and the drainage effect was obviously weakened. On the other hand, the higher viscosity of the liquid film made it more difficult for the gas inside the foam to diffuse outward through the liquid film.[20−23] Therefore, with the increase of temperature, the viscosity of the liquid phase decreased, resulting in a rapid weakening of foamability and foam stability.[24] Moreover, due to the high salinity of formation water in the actual foam drainage gas recovery technology, there were a lot of electrolytes in the foam system.[25,26] When the temperature increased, the irregular movement of these electrolytes in the foam liquid film became increasingly more intense, thus accelerating the drainage effect and making the foam liquid film thin until it finally broke.[27]

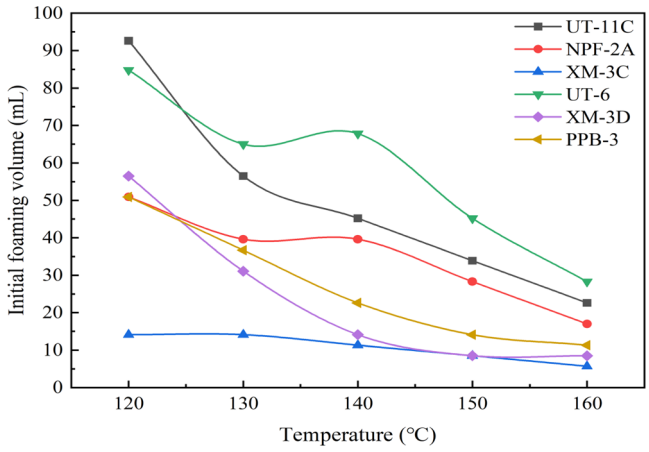

Figure 4. Relationship between initial foaming volume and temperature.

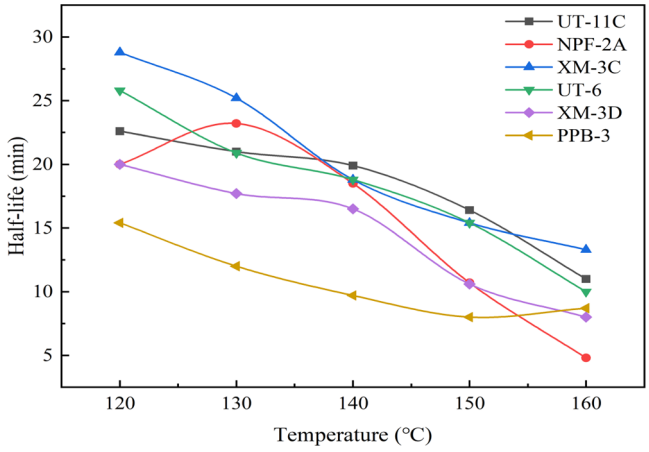

Figure 5. Relationship between half-life and temperature.

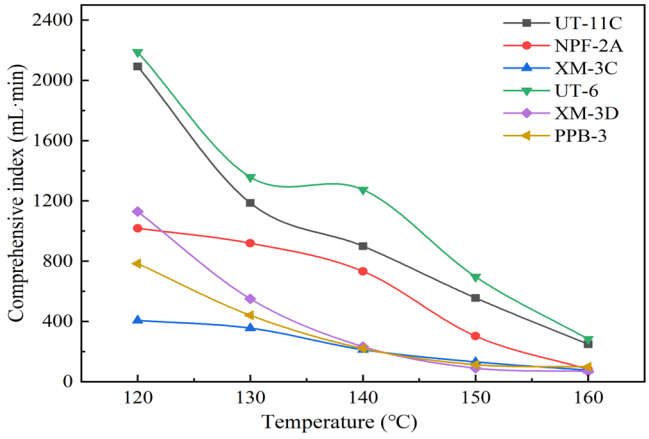

Figure 6. Relationship between comprehensive index and temperature.

Figure 6 shows that the comprehensive indexes of UT-11C and UT-6 were higher than those for the other four at the same temperature, indicating that UT-11C and UT-6 had better temperature resistance than the other four FDAs.

https://doi.org/10.1021/acsomega.2c07715
ACS Omega 2023, 8, 7940−7949

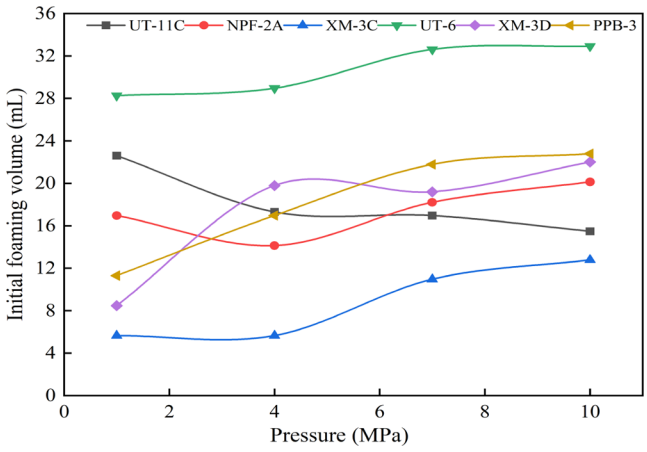

Figure 7. Relationship between initial foaming volume and pressure.

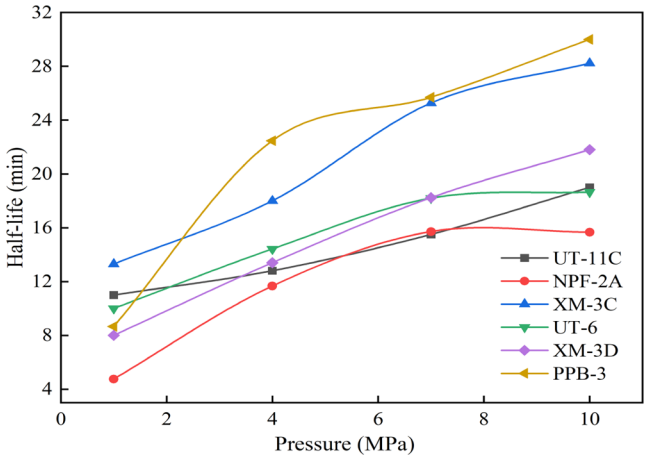

Figure 8. Relationship between half-life and pressure.

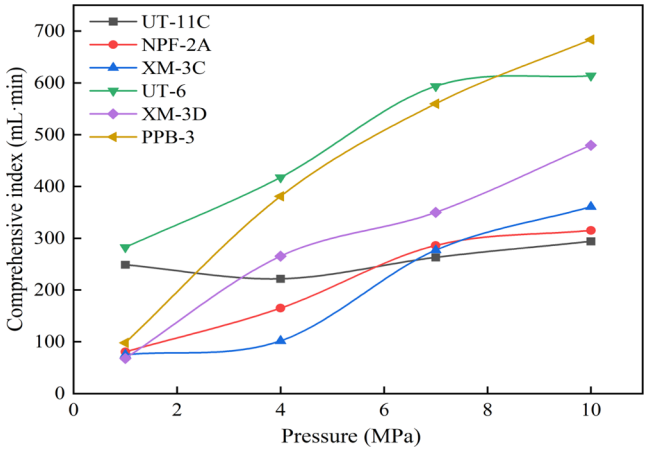

Figure 9. Relationship between comprehensive index and pressure.

3.2. High-Pressure Resistance. The relationship of initial foaming volume, half-life, and comprehensive index with pressure is shown in Figures 7−9, respectively. It could be seen from the figures that with the increase of pressure, the initial foaming volume of FDAs increased except for UT-11C, and the half-life became longer, indicating that the high pressure would strengthen the foamability and foam stability, which was consistent with the classical foam theory.[28] The classical foam theory held that the higher the pressure, the smaller the diameter of a single foam, and the more uniform the foam size.[29] At the same time, the internal friction of the liquid phase increased with the increase of pressure; so, the viscosity of the liquid phase also increased, making the liquid on the foam liquid film difficult to flow and weakening the

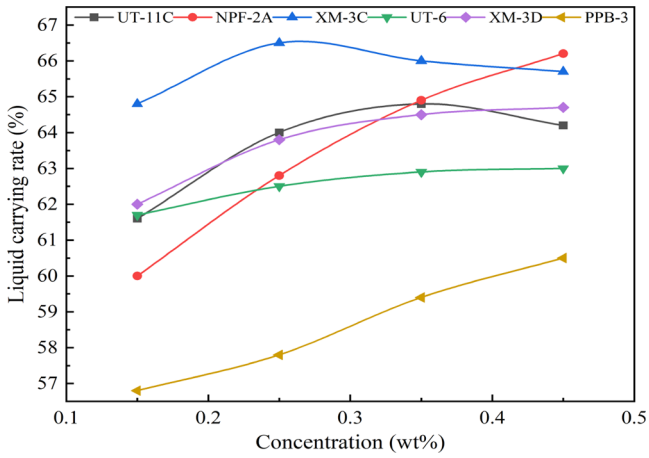

Figure 10. Relationship between liquid carrying rate and concentration when the water−gas ratio was 1:54.

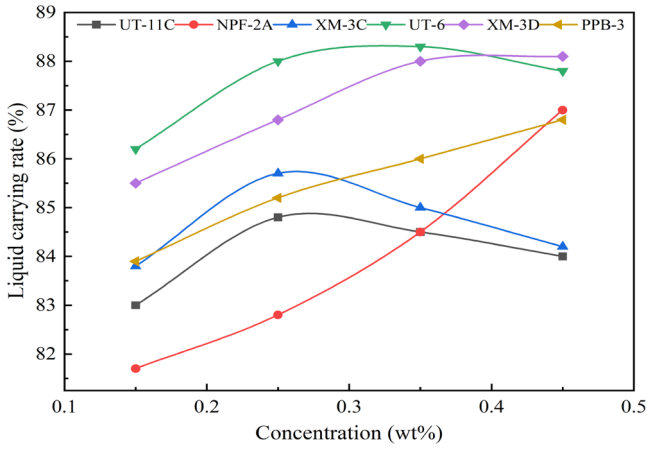

Figure 11. Relationship between liquid carrying rate and concentration when the water−gas ratio was 1:162.

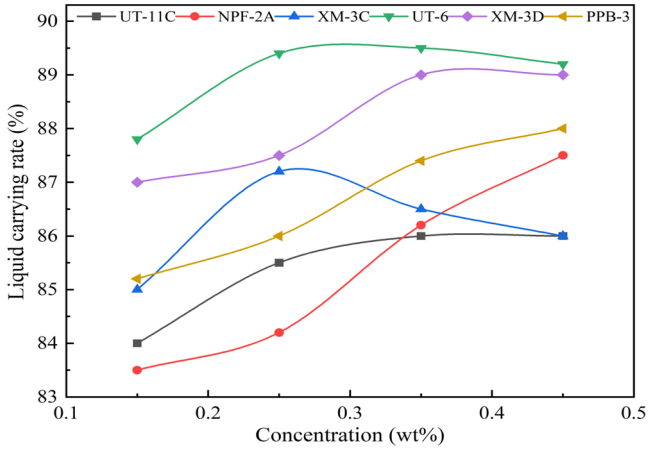

Figure 12. Relationship between liquid carrying rate and concentration when the water−gas ratio was 1:1667.

https://doi.org/10.1021/acsomega.2c07715
ACS Omega 2023, 8, 7940−7949

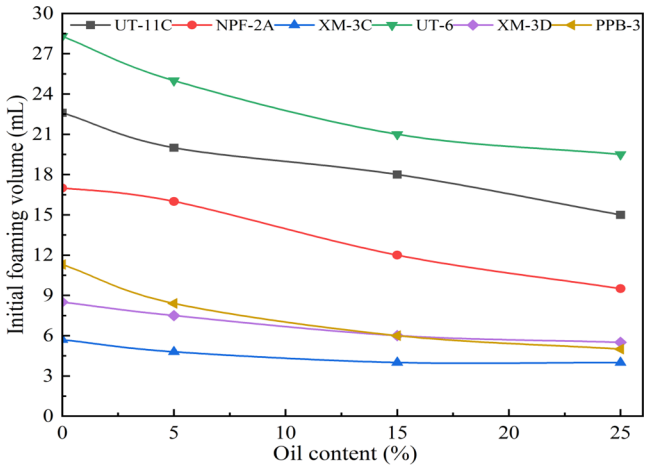

Figure 13. Relationship between initial foaming volume and oil content.

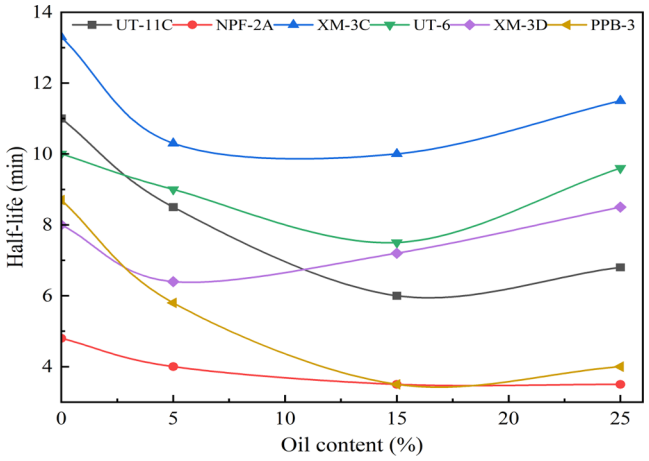

Figure 14. Relationship between half-life and oil content.

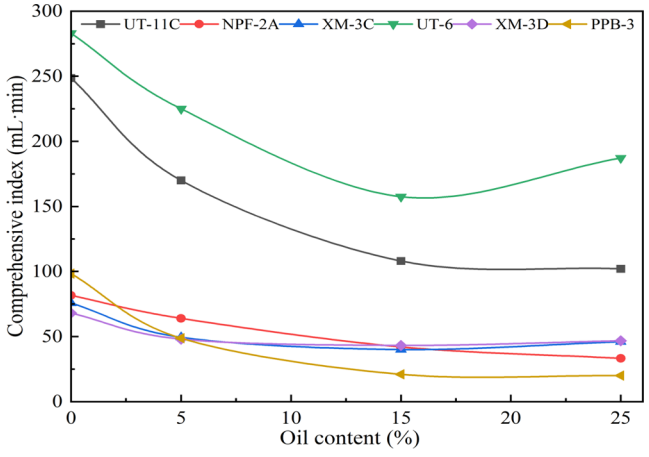

Figure 15. Relationship between comprehensive index and oil content.

drainage effect, and thus the foamability and foam stability were enhanced.[30]

Figure 9 shows that the comprehensive indexes of PPB-3 and UT-6 were higher than those of the other four FDAs at the same pressure, indicating that the foamability and foam

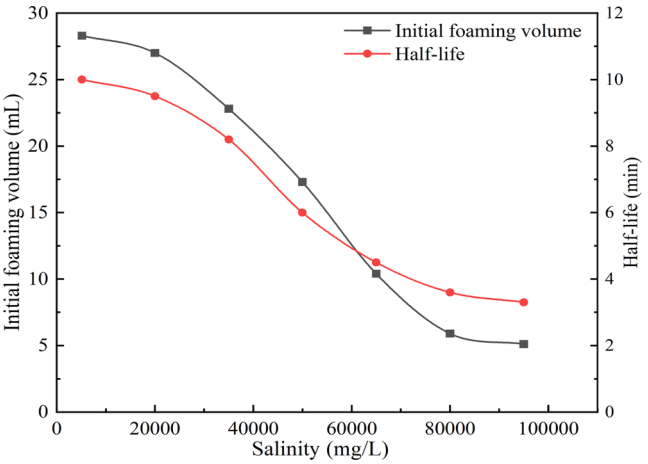

Figure 16. Curves of initial foaming volume and half-life with different salinities.

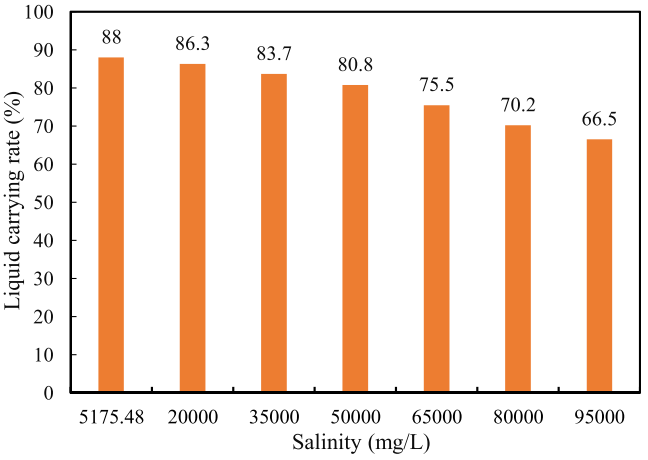

Figure 17. Liquid carrying rates of UT-6 under different salinities.

stability of the two were better than those of the other four FDAs at high pressure.

3.3. Dynamic Liquid Carrying Capacity. The relationship between liquid carrying rates and the concentration under different water−gas ratios is shown in Figures 10−12. Figure 10 shows that when the water−gas ratio was 1:54, the liquid carrying rate of XM-3C was higher than those of the other five at the same concentration. But Figures 11 and 12 show that the liquid carrying rates of UT-6 and XM-3D were higher than those of the other four when the water−gas ratios were 1:162 and 1:1667. However, the difference in liquid carrying rates between UT-6 and XM-3D became more evident when the water−gas ratio was 1:1667. Moreover, according to Figures 11 and 12, the optimum concentration of each FDA could be determined. For example, when the water−gas ratio was 1:162, the liquid carrying rates of UT-6 were 88% at 0.25 wt % and 88.3% at 0.35 wt %, and when the water−gas ratio was 1:1667, the liquid carrying rates of UT-6 were 89.4% at 0.25 wt % and 89.5% at 0.35 wt %. So, for UT-6, the concentration of 0.25 wt % could just meet the actual production needs.

It could also be seen from the figures that with the increase of concentration, the liquid carrying rate first increased and then decreased, or after reaching a certain concentration, it no longer changed with the increasing concentration. On the one hand, when the concentration of FDA was low (lower than the

https://doi.org/10.1021/acsomega.2c07715
ACS Omega 2023, 8, 7940−7949

Figure 18. Images of the bubble on the screen when measuring surface tension: (a) the initial moment; (b) a certain moment in the middle; and (c) the moment for recording.

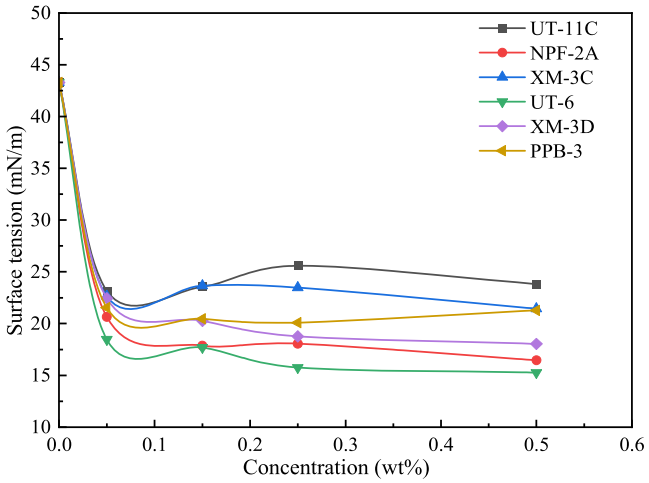

Figure 19. Relationship between surface tension and concentration.

optimal concentration), the liquid carrying capacity was weak because of the small number of surfactant molecules in the solution and weak foamability.[31] On the other hand, when the concentration was high (higher than the optimal concentration), the apparent viscosity of foam increased due to the increasing number of surfactant molecules, generating more relatively stable foams. Therefore, the friction coefficient between foam flow and pipeline increased, so the liquid discharging rate slowed down; finally, the liquid carrying rate decreased or no longer changed with the increase of concentration.[32]

3.4. Oil Resistance. The relationship of initial foaming volume, half-life, and comprehensive index, with the oil content is shown in Figures 13−15, respectively. Among them, the experimental data of no oil content came from the results at 160 °C in high-temperature resistance evaluation.

It could be seen from Figures 13 and 14 that with the increase of oil content, the initial foaming volume decreased, indicating that the increase of oil content would inhibit the foamability; however, the half-life became shorter at first and then longer, indicating that the foam stability became weaker at first and then stronger. The reason was that a small amount of low-viscosity oil acted as a defoamer, which could diffuse and distribute on the foam liquid film, forming an oily film and replacing the original foam liquid film, but the oily film had poor stability and was easy to break, which led to the weakening of foamability and foam stability.[33] As the content of low-viscosity oil continued to increase, the foam stability was enhanced instead of weakened, which was mainly because micelles formed by surfactant molecules could solubilize low-viscosity oil.[34] When the content of low-viscosity oil was greater than a certain value, the low-viscosity oil would be emulsified with the FDA solution, and the oil phase would be emulsified into small oil beads and enter the foam liquid film; so, the emulsion film containing oil beads was formed and wrapped on the foam, making the foam not easy to break, thus improving the foam stability.[35]

As shown in Figure 15, compared with the other four FDAs, UT-6 and UT-11C still had strong foamability and foam stability with the increase of oil content, indicating that UT-6 and UT-11C had stronger oil resistance than the other four FDAs.

3.5. Salinity Resistance. According to the previous screening and evaluation, compared with the other five FDAs, UT-6 still had strong foamability, foam stability, and oil resistance under HTHP. At the same time, UT-6 showed stronger liquid carrying capacity at a lower concentration when it was close to the actual water−gas ratio. Therefore, UT-6 was

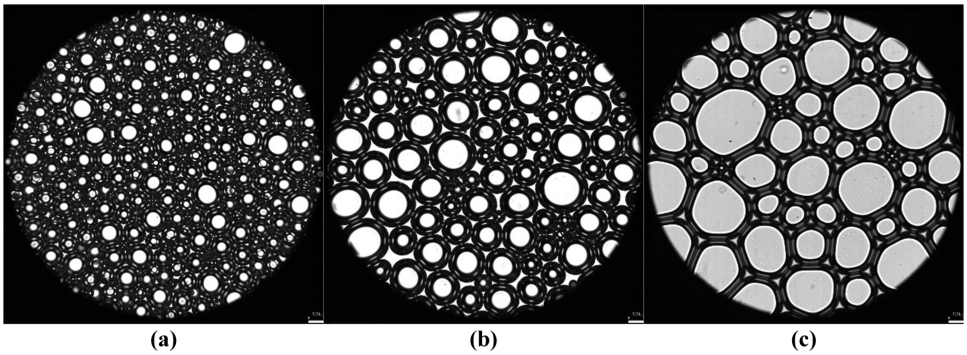

Figure 20. Foam's microscopic morphology of UT-6 at different moments: (a) at the initial moment; (b) at half-life; and (c) at double half-life.

https://doi.org/10.1021/acsomega.2c07715
ACS Omega 2023, 8, 7940−7949

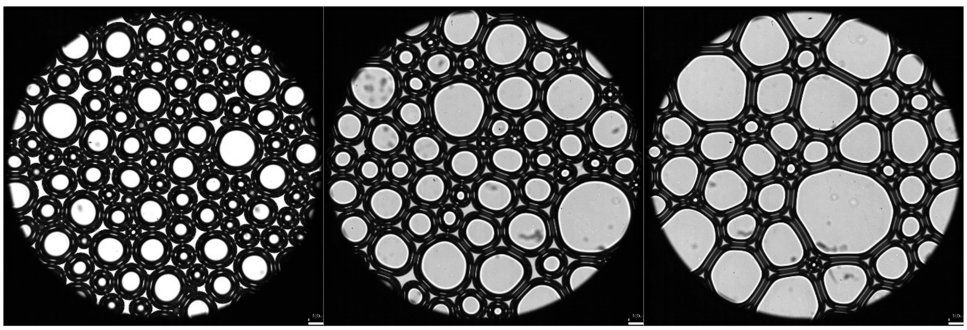

Figure 21. Foam's microscopic morphology of UT-11C at different moments: (a) at the initial moment; (b) at half-life; and (c) at double half-life.

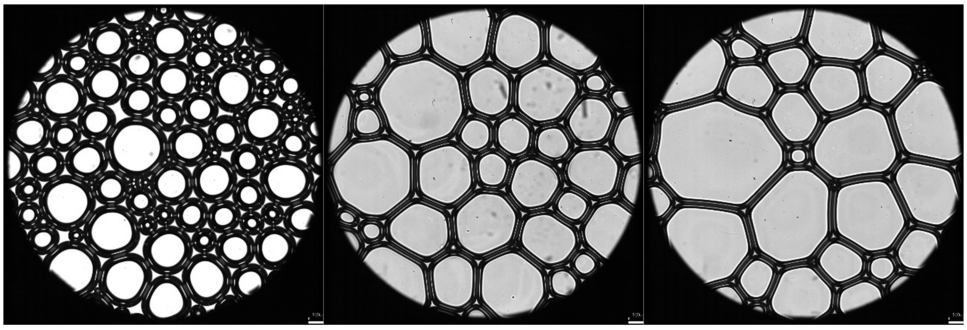

Figure 22. Foam's microscopic morphology of XM-3D at different moments: (a) at the initial moment; (b) at half-life; and (c) at double half-life.

selected for the salinity resistance evaluation. The initial foaming volume and half-life of UT-6 under different salinity conditions were measured, and the experimental results are shown in Figure 16.

As shown in Figure 16, the foamability and foam stability of UT-6 both weakened with the increase of salinity. When the salinity was 5175.48 mg/L, the initial foaming volume and half-life were measured in high-temperature resistance evaluation, which were 28.3mL and 10 min, respectively. But when the salinity increased to 95 000 mg/L, the initial foaming volume and half-life decreased to 5.1 mL and 3.3 min, respectively. The reason was that under the condition of low salinity, the electric double layers on both sides of the foam liquid film could achieve dynamic equilibrium due to the repulsion between the charged groups, which could slow down the thinning speed of the liquid film, so that the foam could maintain a certain degree of stability.[36] However, with the increase of salinity, mineralized ions would weaken the mutual repulsion force between the electric double layers, breaking the original balance, speeding up the liquid loss at the liquid film, and accelerating the thinning speed of the liquid film, resulting in a significant decline in foam stability.[37]

Figure 17 shows that with the increase of salinity, the liquid carrying rate of UT-6 gradually decreased, and when the salinity increased to 80 000 mg/L, the liquid carrying rate of UT-6 could still reach 70.2%, indicating that UT-6 had the liquid carrying capacity to meet the production requirements when the salinity was 80 000 mg/L.[38]

3.6. Surface Tension Reduction Capacity. It could be seen from the screen that the circular bubble gradually lengthened in the axial direction until it became the shape shown in Figure 18c and no longer changed, and the value of surface tension could be recorded.

The relationship between the surface tensions of six FDA solutions and the concentration at 90 °C is shown in Figure 19, which depicts that with the increase of concentration, the surface tension decreased rapidly at first, and the curves tended to be flat when the concentration reached 0.25 wt %. The surface tension of simulated formation water without any FDA was 43.3 mN/m, and after adding a small amount of FDA, the surface tension was greatly reduced, indicating that all six FDAs could reduce the surface tension. However, compared with the other five FDAs, the surface tension of UT-6 was the lowest under the same concentration. For example, when the concentrations were 0.25 and 0.5 wt %, the surface tensions of UT-6 were 15.7 and 15.3 mN/m, respectively. Actually, lowering the surface tension would make the solution easier to foam and easier to be dispersed under the agitation of gas flow.[39] The more dispersed the liquid phase was, the more easily it would be carried out of the wellbore by the gas flow.[40] Therefore, the experimental results obtained in the previous screening and evaluation that UT-6 had strong foamability and strong liquid carrying capacity at high temperatures were verified by surface tension measurement.

3.7. Morphology under an Electron Microscope. To highlight the difference in foam microscopic morphology among different FDAs after foaming, according to the results of previous experiments, three FDAs with relatively good performance were selected for morphology study under an electron microscope, namely, UT-6, UT-11C, and XM-3D, and their foam's microscopic morphologies are shown in Figures 20−22, respectively.

It could be seen from the figures that at the initial moment, the bubbles of UT-6 were closely arranged, with the largest number and the smallest single bubble size, while the initial bubbles of UT-11C and XM-3D were relatively big and loosely arranged, which confirmed UT-6's strong foamability. At half-

https://doi.org/10.1021/acsomega.2c07715
ACS Omega 2023, 8, 7940−7949

life, the bubble arrangement of UT-6 was still relatively tight and uniform; however, for UT-11C and XM-3D, many larger bubbles appeared. According to plateau boundary theory, the internal pressure of small bubbles was higher than that of large bubbles because of their small inner diameter, so the gas inside the small bubbles would continuously diffuse into the large bubbles through the liquid film, making small bubbles smaller and smaller until they finally disappeared. Therefore, the appearance of large bubbles meant that the defoaming speed was accelerated.[41] At double half-life, the foam's microscopic morphology was almost dominated by large-sized bubbles; however, the foam liquid film of UT-6 still had a certain thickness, and the drainage speed at the plateau boundary was relatively slow. Therefore, the observation results of microscopic morphology also confirmed UT-6's strong foam stability.

4. CONCLUSIONS

Based on the actual formation conditions, a HTHP evaluation device for FDA was set up in this study. The key performance of six FDAs, such as HTHP resistance, dynamic liquid carrying capacity, oil resistance, and salinity resistance, was evaluated systematically. Taking initial foaming volume, half-life, comprehensive index, and liquid carrying rate as evaluation indexes, the FDA with the best performance was screened out and the concentration was optimized. In addition, the experimental results were verified by surface tension measurement and electron microscopy observation. The experimental conclusions are as follows:

(1) The sulfonate compound surfactant (UT-6) had good foamability, excellent foam stability, and better oil resistance at high temperature and high pressure.
(2) UT-6 had stronger liquid carrying capacity at a lower concentration, which could meet the production requirement when the salinity was 80 000 mg/L.
(3) Compared with the other five FDAs, UT-6 was more suitable for HTHP gas wells in block X of the Bohai Bay Basin, whose optimal concentration was 0.25 wt %.
(4) UT-6 solution had the lowest surface tension at the same concentration, whose generated bubbles were closely arranged and uniform in size. Moreover, in UT-6's foam system, the drainage speed at the plateau boundary was relatively slower with the smallest bubble.

AUTHOR INFORMATION

Corresponding Author

Lihao Liang − *Research Institute of Petroleum Exploration & Development, Beijing 100083, People's Republic of China;* orcid.org/0000-0003-1869-9481; Phone: 010-83592072; Email: Petrolihao@163.com

Authors

Jian Guan − *School of Petroleum Engineering, China University of Petroleum (East China), Qingdao 266580 Shandong, People's Republic of China;* orcid.org/0000-0001-8664-3389

Yulong Zhao − *School of Petroleum Engineering, China University of Petroleum (Beijing), Beijing 102249, People's Republic of China*

Ning Sun − *School of Petroleum Engineering, China University of Petroleum (East China), Qingdao 266580 Shandong, People's Republic of China*

Wei Lu − *PetroChina Company Limited, Huanqing Oil Production Factory of Yumen Oilfield Co., Ltd., Qingyang 745700, People's Republic of China*

Yuanshui Zhen − *PetroChina Company Limited, Research Institute of Exploration and Development of Yumen Oilfield Co., Ltd., Jiuquan 735019, People's Republic of China*

Complete contact information is available at: https://pubs.acs.org/10.1021/acsomega.2c07715

Funding

This work was supported by Central Program of Basic Science of the National Natural Science Foundation of China (grant no.: 72088101) and Structure and Evolution Mechanism of Microscopic Fracture induced by CO_2 Hybrid Fracturing in Shale Oil Reservoir (grant no.: 52274058).

Notes

The authors declare no competing financial interest.

ACKNOWLEDGMENTS

The authors thank Prof. Dr. Caili Dai and her group and Prof. Dr. Shaoran Ren and his group in China University of Petroleum (East China) for providing the necessary facilities and technical support.

REFERENCES

(1) Karakashev, S. I.; Nguyen, P. T.; Tsekov, R.; Hampton, M. A.; Nguyen, A. V. Anomalous ion effects on rupture and lifetime of aqueous foam films formed from monovalent salt solutions up to saturation concentration. *Langmuir* **2008**, *24*, 11587−11591.
(2) Kamal, M. S.; Shakil, H. M.; Fogang, L. T. A Zwitterionic Surfactant Bearing Unsaturated Tail for Enhanced Oil Recovery in High-Temperature High-Salinity Reservoirs. *J. Surfactants Deterg.* **2018**, *21*, 165−174.
(3) Yang, L.; Hongkui, G.; Xian, S.; Yuanfang, C.; Kunheng, Z.; Hao, C.; Yinghao, S.; Junjing, Z.; Xiangmei, Q. The effect of microstructure and rock mineralogy on water imbibition characteristics in tight reservoirs. *J. Nat. Gas Sci. Eng.* **2016**, *34*, 1461−1471.
(4) Ge, H.-K.; Liu, Y.; Yinghao, S.; Kai, R.; Fanbao, M.; Wenming, J.; Shan, W. Experimental investigation of shale imbibition capacity and the factors influencing loss of hydraulic fracturing fluids. *Pet. Sci.* **2015**, *12*, 636−650.
(5) Kamal, M. A Novel Approach to Stabilize Foam Using Fluorinated Surfactants. *Energies* **2019**, *12*, No. 1163.
(6) Chunsheng, W.; Xiaohu, W.; Qiuying, D.; Bingkai, F.; Chang, X. The Mechanism Study of Vortex Tools Drainage Gas Recovery of Gas Well. *Adv. Pet. Explor. Dev.* **2014**, *7*, 62−66.
(7) Huang, B.; Xiaohan, N.; Cheng, F.; Wanfu, Z.; Siqiang, F.; Tingwei, Z. Study on foam transport mechanism and influencing factors in foam drainage gas recovery of natural gas well. *J. Dispersion Sci. Technol.* **2022**, *43*, 2049−2057.
(8) Haiwen, W.; Changjiang, L. Process parameters design method of drainage gas recovery technology in gas-driven pump for coalbed methane production. *J. Pet. Sci. Eng.* **2021**, *207*, No. 109167.
(9) Yinghao, S.; Guohua, L.; Hongkui, G.; Xinyu, Y.; Qian, L.; Xuejing, G. Optimization of coiled-tubing drainage gas recovery technology in tight gas field. *Adv. Mech. Eng.* **2017**, *9*, No. 1687814017711333.
(10) Wang, Q.; Shenglai, Y.; Haishui, H.; Lu, W.; Kun, Q.; Jieqiong, P. Experimental Investigation on the Effects of CO_2 Displacement Methods on Petrophysical Property Changes of Ultra-Low Permeability Sandstone Reservoirs Near Injection Wells. *Energies* **2019**, *12*, No. 327.
(11) Tan, X.-H.; Xiaoping, L.; Jianyi, L. Model of continuous liquid removal from gas wells by droplet diameter estimation. *J. Nat. Gas Sci. Eng.* **2013**, *15*, 8−13.

(12) Daghlian Sofla, S. J.; Mohammad, S.; Abdolhossein, H. S. Toward mechanistic understanding of natural surfactant flooding in enhanced oil recovery processes: The role of salinity, surfactant concentration and rock type. *J. Mol. Liq.* **2016**, *222*, 632−639.
(13) Durand, M.; Langevin, D. Physicochemical approach to the theory of foam drainage. *Eur. Phys. J. E* **2002**, *7*, 35−44.
(14) Rio, E.; Wiebke, D.; Anniina, S.; Dominique, L. Unusually stable liquid foams. *Adv. Colloid Interface Sci.* **2014**, *205*, 74−86.
(15) Telmadarreie, A.; Japan, J. T. Static and Dynamic Performance of Wet Foam and Polymer-Enhanced Foam in the Presence of Heavy Oil. *Colloids Interfaces* **2018**, *2*, No. 38.
(16) Yang, L.; Shuo, W.; Qingping, J.; Yuan, Y.; Jian, G. Effects of microstructure and rock mineralogy on movable fluid saturation in tight reservoirs. *Energy Fuels* **2020**, *34*, 14515−14526.
(17) Sakai, T.; Youhei, K. The Effect of Some Foam Boosters on the Foamability and Foam Stability of Anionic Systems. *J. Surfactants Deterg.* **2004**, *7*, 291−295.
(18) Arnaudov, L.; Nikolai, D. D.; Irena, S.; Patrick, D.; Guy, B.; Ammanuel, M. Effect of Oily Additives on Foamability and Foam Stability. 1. Role of Interfacial Properties. *Langmuir* **2001**, *17*, 6999−7010.
(19) Xue, Y.; Guang, Z.; Caili, D.; Yining, W.; Yahui, L. Interfacial characteristics and the stability mechanism of a dispersed particle gel (DPG) three-phase foam. *J. Mol. Liq.* **2020**, *301*, No. 112425.
(20) Yekeen, N.; Muhammad, A. M.; Idris, A. K.; Padmanabhan, E.; Junin, R.; et al. A comprehensive review of experimental studies of nanoparticles-stabilized foam for enhanced oil recovery. *J. Pet. Sci. Eng.* **2018**, *164*, 43−74.
(21) Pandey, S.; Rahul, P. B.; Dinesh, O. S. Effect of counterions on surface and foaming properties of dodecyl sulfate. *J. Colloid Interface Sci.* **2003**, *267*, 160−166.
(22) Yekeen, N.; Idris, A. K.; Manan, M. A.; Samin, A. M.; Risal, A. R.; Kun, T. X. Bulk and bubble-scale experimental studies of influence of nanoparticles on foam stability. *Chin. J. Chem. Eng.* **2016**, *25*, 347−357.
(23) AlYousef, Z. A.; Mohammed, A. A.; David, S. S. The effect of nanoparticle aggregation on surfactant foam stability. *J. Colloid Interface Sci.* **2018**, *511*, 365−373.
(24) Stocco, A.; Drenckhan, W.; Rio, E.; Langevin, D.; Binks, B. P. Particle-stabilized foams: an interfacial study. *Soft Matter* **2009**, *5*, 2215−2222.
(25) Sakthivel, S.; Salin, R. B. Imidazolium based ionic liquid stabilized foams for conformance control: bulk and porous scale investigation. *RSC Adv.* **2021**, *11*, 29711−29727.
(26) Hanamertani, A. S.; Rashidah, M. P.; Ninie, A. M.; Mibrahim, A. M. The use of ionic liquids as additive to stabilize surfactant foam for mobility control application. *J. Pet. Sci. Eng.* **2018**, *167*, 192−201.
(27) Czakaj, A.; Kannan, A.; Wiśniewska, A.; Grześ, G.; Krzan, M.; Warszyński, P.; Fuller, G. G. Viscoelastic interfaces comprising of cellulose nanocrystals and lauroyl ethyl arginate for enhanced foam stability. *Soft Matter* **2020**, *16*, 3981−3990.
(28) Hamza, M. F.; Hassan, S.; Zulkifli, M. M.; Chandra, M. S.; Karl, D. S.; Abdelazeem, A. A. Nano-fluid viscosity screening and study of in situ foam pressure buildup at high-temperature high-pressure conditions. *J. Pet. Explor. Prod. Technol.* **2020**, *10*, 1115−1126.
(29) Zhang, C.; Peng, W.; Guoliang, S. Study on enhanced oil recovery by multi-component foam flooding. *J. Pet. Sci. Eng.* **2019**, *177*, 181−187.
(30) Liang, S.; Shaoquan, H.; Jie, L.; Guorui, X.; Bo, Z.; Yudong, Z.; Hua, Y.; Jianye, L. Study on EOR method in offshore oilfield: Combination of polymer microspheres flooding and nitrogen foam flooding. *J. Pet. Sci. Eng.* **2019**, *178*, 629−639.
(31) Zhao, H.; Chengxuan, H.; Yawen, Z.; Jian, Y.; Cong, L.; Baocai, X. Study on foaming properties of N-acyl amino acid surfactants: Sodium N-acyl glycinate and sodium N-acyl phenylalaninate. *Colloids Surf., A* **2019**, *567*, 240−248.
(32) Varade, S. R.; Ghosh, P. Foaming in aqueous solutions of zwitterionic surfactant in presence of monovalent salts: The specific ion effect. *Chem. Eng. Commun.* **2020**, *207*, 1216−1233.
(33) Duan, X.; Jirui, H.; Tingting, C.; et al. Evaluation of oil-tolerant foam for enhanced oil recovery: Laboratory study of a system of oil-tolerant foaming agents. *J. Pet. Sci. Eng.* **2014**, *122*, 428−438.
(34) Nesterenko, A.; Audrey, D.; Huiling, L.; Danièle, C.; Isabelle, P. Influence of a mixed particle/surfactant emulsifier system on water-in-oil emulsion stability. *Colloids Surf., A* **2014**, *457*, 49−57.
(35) Sun, S.; Yan, W.; Congtai, Y.; Hongbing, W.; Wendong, W.; Jianhui, L.; Chunling, L.; Songqing, H. Tunable stability of oil-containing foam systems with different concentrations of SDS and hydrophobic silica nanoparticles. *J. Ind. Eng. Chem.* **2020**, *82*, 333−340.
(36) Maestro, A.; Rio, E.; Drenckhan, W.; Langevin, D.; Salonen, A. Foams stabilized by mixtures of nanoparticles and oppositely charged surfactants: relationship between bubble shrinkage and foam coarsening. *Soft Matter* **2014**, *10*, 6975−6983.
(37) Rudyk, S.; Al Khamisi, S.; Al Wahaibi, Y. Effects of water salinity on the foam dynamics for EOR application. *J. Pet. Explor. Prod. Technol.* **2021**, *11*, 3321−3332.
(38) Hadian Nasr, N.; Syed, M. M.; Saeed, A.; Hamed, H. A comparison of foam stability at varying salinities and surfactant concentrations using bulk foam tests and sand pack flooding. *J. Pet. Explor. Prod. Technol.* **2020**, *10*, 271−282.
(39) Chuncheng, L.; Yinghui, L.; Hui, P. Molecular simulation study of interfacial tension reduction and oil detachment in nanochannels by surface-modified silica nanoparticles. *Fuel* **2021**, *292*, No. 120318.
(40) Behera, M. R.; Shailesh, R. V.; Pallab, G.; Pintu, P.; Ajay, S. N. Foaming in Micellar Solutions: Effects of Surfactant, Salt, and Oil Concentrations. *Ind. Eng. Chem. Res.* **2014**, *53*, 18497−18507.
(41) Kumar, A.; Patham, B.; Mohanty, S.; Nayak, S. K. Polypropylene−nano-silica nanocomposite foams: mechanisms underlying foamability, foam microstructure, crystallinity and mechanical properties. *Polym. Int.* **2020**, *69*, 373−386.

https://doi.org/10.1021/acsomega.2c07715
ACS Omega 2023, 8, 7940−7949